Review

Nanotube Membrane Based Biosensors

*Punit Kohli, Marc Wirtz, Charles R. Martin**

Department of Chemistry and Center for Bio/Nano Interface, University of Florida, Gainesville, Florida, USA
*e-mail: crmartin@chem.ufl.edu

Received: May 19, 2003
Final version: July 15, 2003

Abstract
We review highly sensitive detection based on electrochemical methods. These methods are based on monodisperse gold and alumina nanotubule membranes with inside diameter approaching molecular dimensions. The analyte species can be detected by measuring a change in trans-membrane current when the analyte is added to the nanotubule-based cell. The second method entails the use of a concentration change based on the nanotubule membrane. Biomemtic ion-gated channels micropore and nanotubule membrane sensors are also reviewed. These synthetic ion channels can be switched from an "off" state to an "on" state in response to an external chemical stimulus. Using these methods, we have achieved detection limits as low as 10 pM. Potential applications for these biosensors are in fields such as bioanalytical, biomedical, pharmaceutical and drug discovery.

Keywords: Gold nanotubes, Alumina membranes, Nanotube membranes, Template synthesis, Electroless deposition, Molecular sieves, Resistive sensing, Ion channel mimetics

1. Introduction

In this mini-review, we discuss abiotic nanotubule membranes for biomimetic ion channels and sensing applications. The membranes are composed of either gold or alumina nanotubules. The gold nanotubule membranes are prepared via electroless deposition of Au onto the pore walls of a polycarbonate membrane; i.e., the pores act as templates for the nanotubes. The use of these membranes in new approaches to electrochemical sensing is discussed. In this case, a current is forced through the nanotubes, and analyte molecules present in a contacting solution phase modulate the value of this transmembrane current (Figure 1a). We also discuss synthetic micropore and nanotubule membranes that mimic the function of a ligand-gated ion channel; i.e., these membranes can be switched from an "off" state (no or low ion-current through the membrane) to an "on" state (higher ion-current) in response to the presence of a chemical stimulus, i.e., drug or surfactant (Figure 1b). Ion-channel mimetic membranes discussed here are based on both modified Au-nanotube and microporous alumina membranes.

2. Nanotube Membranes

We have been exploring the transport and electrochemical properties of nanotube membranes prepared by the template method [1–3], a general approach for preparing nanomaterials. This method entails synthesis or deposition of the desired material within the cylindrical and monodisperse pores of a nanopore membrane or other solid. We have used polycarbonate filters, prepared via the track-etch method [4], and nanopore aluminas, prepared electrochemically from Al foil [5], as our template materials. Cylindrical nanostructures with monodisperse diameters and lengths are obtained, and depending on the membrane and synthetic method used, these may be solid nanowires or hollow nanotubes. We, and others, have used this method to prepare nanowires and tubes composed of metals [5–12], polymers [13–15], semiconductors [16, 17], carbons [18–19], and Li^+ intercalation materials [20–22]. It is also possible to prepare composite nanostructures, both concentric tubular composites, where an outer tube of one material surrounds an inner tube of another [23, 24], and segmented composite nanowires [25].

One application for these nanotube membranes is in electroanalytical chemistry where the membrane is used to sense analyte species [26, 27]. In that work, membranes containing gold nanotubes with inside diameters that approached molecular dimensions (1 nm to 4 nm) were used [26]. The Au nanotube membrane was placed between two salt solutions and a constant transmembrane potential was applied. The resulting transmembrane current, associated with migration of ions through the nanotubes, was measured. When an analyte molecule whose diameter was comparable to the inside diameter of the nanotubes was added to one salt solution, this molecule partitioned into the nanotubes and partially occluded the pathway for ion transport. This resulted in a decrease in the transmembrane ion current, and the magnitude of the drop in current was found to be proportional to the concentration of the analyte [26].

In the experiment discussed above, a baseline transmembrane ion current was established, and the analyte molecule, in essence, turned off this current. It occurred to us that there might be an advantage in doing the opposite;

  DOI: 10.1002/elan.200302916

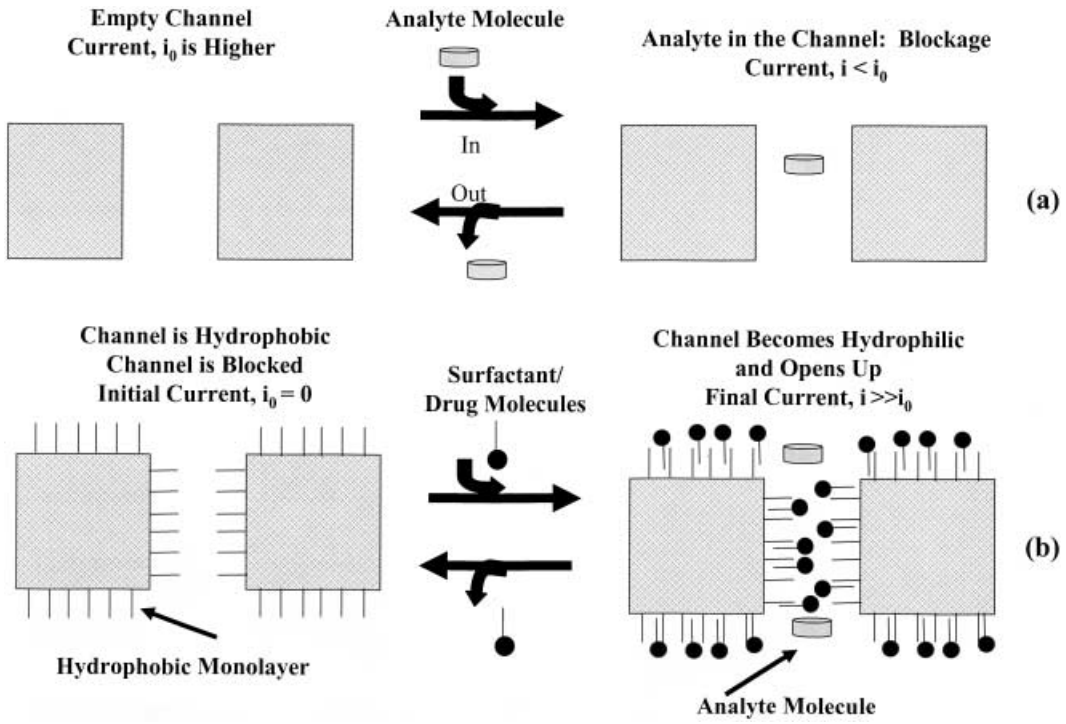

Fig. 1. Schematic of electrochemical methods described in the article. a) The analyte species is detected by measuring the change in trans-membrane current when the analyte is added to the nanotubule-based cell. b) The ligand-gated mimetic ion-channel configuration: Following the addition of an external stimulus (a surfactant or a drug molecule in our case), the ion-channel opens up. This is detected by an increase in the current across the abiotic membrane.

i.e., starting with an ideally zero current situation and having the analyte molecule switch on the ion current. That is, we would like to make a synthetic membrane that mimics the function of a ligand-gated ion channel. An example is the acetylcholine-gated ion channel [28], which is closed ("off" state) in the absence of acetylcholine but opens (and supports an ion current, "on" state) when acetylcholine binds to the channel. In order to accomplish this, the off state was obtained by making gold and alumina membranes hydrophobic, and the on state was obtained by introducing ions and electrolyte into the membrane [29]. Ions were introduced by either partitioning a hydrophobic ionic species (e.g., a drug or a surfactant) into the membrane.

3. Membrane Preparation and Analysis

Commercially-available "track-etched" polycarbonate filters are used as the templates to prepare the Au nanotubes. The track-etch process [4] entails bombarding a solid material (in this case a ca. 10 μm-thick polycarbonate film) with a collimated beam of high-energy nuclear fission fragments to create parallel damage tracks in the film. The damage tracks are then etched into monodisperse cylindrical pores by exposing the film to a concentrated solution of aqueous base. The diameter of the pores is determined by the etch time and the etch-solution temperature. Membranes with pore diameters ranging from as small as 10 nm to as large as ca. 10 μm are available commercially. The membranes used for these studies had nominal pore diameters of 30 nm and contained 6×10^8 pores per cm^2 of membrane surface area.

The electroless plating method used to deposit the Au nanotubes [7, 30] within the pores of these membranes. Briefly, the template membrane is first "sensitized" by immersion into a $SnCl_2$ solution which results in deposition of Sn(II) onto all of the membrane's surfaces (pore walls and membrane faces). The sensitized membrane is then immersed into a $AgNO_3$ solution, and a surface redox reaction occurs (Equation 1) which yields nanoscopic metallic Ag particles on the membrane surfaces.

$$Sn(II)_{surf} + 2Ag(I)_{aq} \rightarrow Sn(IV)_{surf} + 2Ag(0)_{surf} \quad (1)$$

(The subscripts surf and aq denote species adsorbed to the membrane surfaces and species dissolved in solution, respectively.) The membrane is then immersed into a commercial gold plating solution and a second surface redox reaction occurs, to yield Au nanoparticles on the surfaces (Equation 2).

$$Au(I)_{aq} + Ag(0)_{surf} \rightarrow Au(0)_{surf} + Ag(I)_{aq} \quad (2)$$

These surface-bound Au nanoparticles are good autocatalysts for the reduction of Au(I) to Au(0) using formaldehyde as the reducing agent. As a result, Au deposition begins at the pore walls, and Au tubes are obtained within the pores [7, 9, 30, 31].

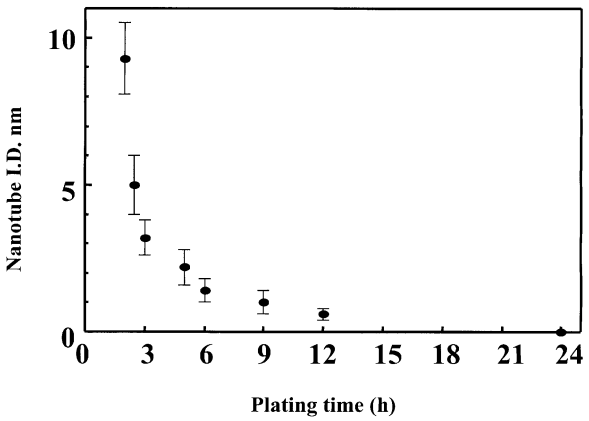

Fig. 2. Variation of the nanotube effective inside diameter with plating time.

3.1. Estimation of the Nanotube inside Diameter

We use a gas-transport method to obtain an estimate of the inside diameter (i.d.) of the template-synthesized Au nanotubes [7]. Briefly, the tube-containing membrane is placed in a gas-permeation cell, and the upper and lower half-cells are evacuated. The upper half-cell is then pressurized, typically to 20 psi with H_2, and the pressure-time transient associated with leakage of H_2 through the nanotubes is measured using a pressure transducer in the lower half-cell. The pressure-time transient is converted to gas flux (Q, mol s^{-1}) which is related to the radius of the nanotubes (r, cm) via [7]

$$Q = 4/3(2\pi/MRT)^{1/2}(nr^3\Delta P/l) \quad (3)$$

where ΔP is the pressure difference across the membrane (dynes cm^{-2}), M is the molecular weight of the gas, R is the gas constant (erg K^{-1} mol^{-1}), n is the number of nanotubes in the membrane sample, l is the membrane thickness (cm) and T is the temperature (K). At long plating times, membranes containing nanotubes with i.d.s of molecular dimensions are obtained (Figure 2).

4. Chemical Sensing with the Au Nanotube Membranes

These Au nanotube membranes have been used as sensors for the determination of ultratrace concentrations of ions and molecules [26, 27a]. In this case, the nanotube membrane was allowed to separate two salt solutions, a constant transmembrane potential was applied, and the resulting transmembrane current was measured. When an analyte of comparable dimensions to the inside diameter of the nanotubes was added to one of the salt solutions, a decrease in transmembrane current was observed (Figure 1a). The magnitude of this drop in transmembrane current (Δi) is proportional to the analyte concentration.

The use of gold and alumina nanotubule membranes for separation of proteins is also recently reported [27b and c]. The factors which affect the selectivity and sensitivity of protein transport in PEG-thiol-treated gold nanotube discussed are internal diameter of nanotubes, pH of the solution, and applied transmembrane potential membranes [27b]. The transport properties of four proteins (lysozyme, bovine serum albumin, carbonic anhydrase, and bovine hemoglobulin) of differing sizes and pI values were investigated. In general, membranes containing larger diameter nanotubes showed higher fluxes and lower selectivities than membranes with smaller diameter nanotubes. Transmembrane electrophoresis can be used to augment the diffusive transport selectivity. For example, for proteins that are oppositely charged, a combination of a large transmembrane potential and a large nanotube diameter can be used to optimize both selectivity and flux. In addition to transmembrane potential and nanotube diameter, solution pH value plays an important role in determining the transport selectivity. This is because pH determines the net charge on the protein molecule and this, in turn, determines the importance of the electrophoretic transport term.

5. Calibration Plots and Detection Limits

As in the transport experiments, a U-tube cell was assembled with the nanotube membrane separating the two halves of the cell. The two half-cells were filled with the desired electrolyte and an electrode was placed into each half-cell. Three different sets of electrodes and electrolytes were used. The first set consisted of two Pt plate electrodes, and the electrolyte used in both half-cells was 0.1 M KF. The second set consisted of two Ag/AgCl wires, and the electrolyte used in both half-cells was 0.1 M KCl. The third set consisted of two Ag/AgI wires immersed in 0.1 M KI.

As noted above, the experimental protocol used with these cells was to immerse the electrodes into the appropriate electrolyte and apply a constant potential between the electrodes. The resulting transmembrane current was measured and recorded on an X-t recorder. After obtaining this baseline current, the anode half-cell was spiked with a known quantity of the desired analyte (Figures 1a and 3). This resulted in a change in the transmembrane current, Δi (Figure 4). A potentiostat was used to apply the potential between the electrodes and measure the transmembrane current. The transmembrane potential used was on the order of 0.5 V [26, 27].

Plots of log Δi vs. log[analyte] for the analytes $Ru(bpy)_3^{2+}$, MV^{2+} and quinine (Figure 3) were obtained using Ag/AgCl electrodes and 0.1 M KCl as the electrolyte in both half-cells (Figure 5). For these experiments, a membrane with 2.8 nm i.d. Au nanotubes was used. A log-log format is used for these "calibration plots" because of the large dynamic range (spanning as much as five orders of magnitude in analyte concentration) obtained with this cell. Analogous calibration plots were obtained for the other electrode/electrolyte systems investigated. The detection limits [26] obtained are shown in Table 1. For the divalent cationic electrolytes, the detection limits were lowest (best) in the Ag/AgI/KI cell and

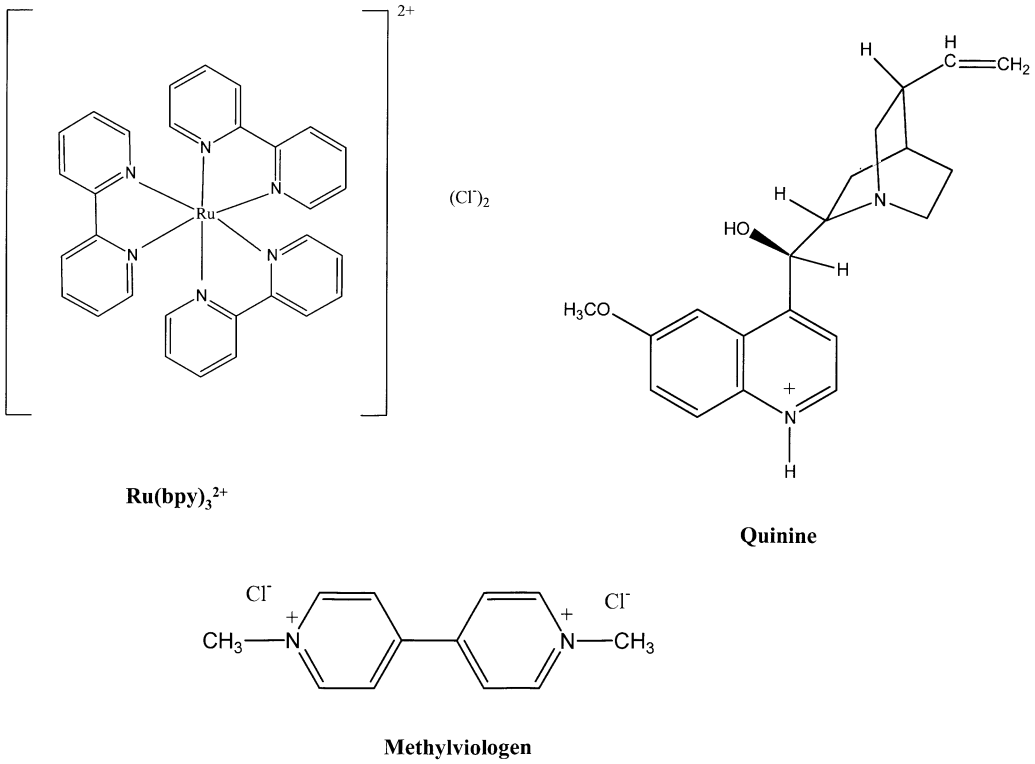

Fig. 3. Chemical structures and approximate relative sizes of the three "big molecule/small molecule" pairs used in the molecular filtration experiments. Quinine, MV^{2+}, and $Ru(bpy)_3^{2+}$ were also used as analytes in the sensor work.

worst in the Pt/KF cell. The detection limit for quinine was the same in both the Ag/AgI/KI and Ag/AgCl/KCl cells. In general, the detection limit decreases as the size of the analyte molecule increases (see Figure 3). Finally, the detection limits obtained (down to 10^{-11} M) are extraordinary and compete with even the most sensitive of modern analytical methods.

The majority of the quinine in both the KCl and KI solutions is present as the monoprotonated (monocationic)

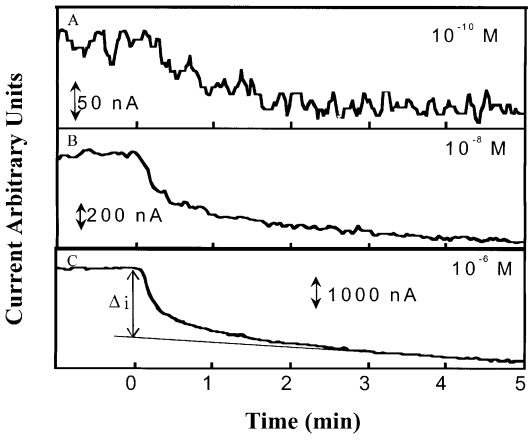

Fig. 4. Nanotube membrane sensor current-time transients associated with spiking the anode half cell with the indicated concentrations of $Ru(bpy)_3^{2+}$. Tube i.d. = 2.8 nm; Ag/AgCl/KCl cell: Δi determined as shown in C.

form. Perhaps the reason the detection limits for $Ru(bpy)_3^{2+}$ and MV^{2+} are lower in the Ag/AgI/KI cell while the detection limit for quinine is the same in both this cell and the Ag/AgCl/KCl cell has to do with the difference in charge of these analytes (predominately monocationic vs. dicationic). To explore this point, the detection limits for a neutral analyte, 2-naphthol, were obtained in both the Ag/AgI/KI and Ag/AgCl/KCl cells. Like quinine, the detection limit for this neutral analyte was the same in both cells (10^{-6} M, Table 1).

In the membrane transport studies it was shown that $Ru(bpy)_3^{2+}$ and MV^{2+} come across such membranes as the ion multiples $Ru(bpy)_3^{2+}(X^-)_2$ and $MV^{2+}(X^-)_2$ (X^- = anion) [7]. In the KI cell, the ion multiple contains two larger (relative to chloride) iodide anions. Perhaps the larger size of the iodide ion multiple accounts for the lower detection limit in the KI-containing cell. If this is true then the difference between the quinine cation paired with one I^- vs. this cation paired with one Cl^- is not great enough to cause the detection limit for this predominately monovalent analyte to be significantly different in the Ag/AgI/KI vs. the Ag/AgCl/KCl cells (Table 1).

The final variable to be investigated is the effect of nanotube inside diameter on detection limit. To explore this parameter, membranes with nanotube inside diameters of approximately of 3.8, 2.8, 2.2, 1.8, and 1.4 nm were prepared and used in the Ag/AgI/KI cell [26]. Calibration plots for the analytes $Ru(bpy)_3^{2+}$, MV^{2+}, and quinine were generated as before, and detection limits were obtained from these

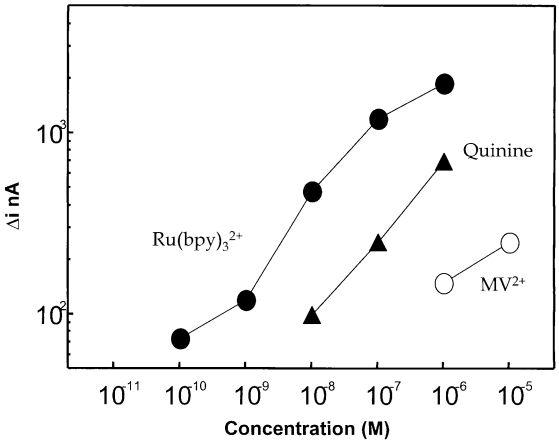

Fig. 5. Calibration plots for the indicated analytes. Membrane and cell as described in Figure 3.

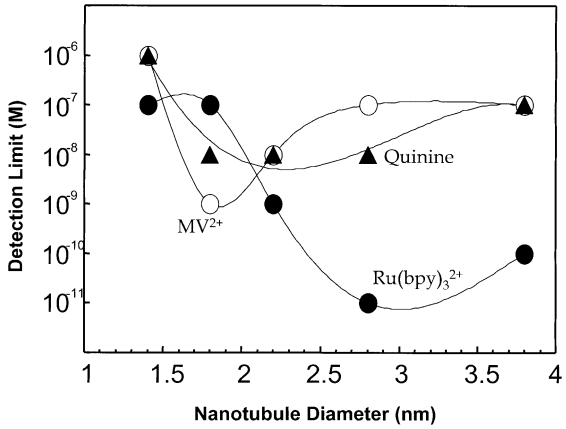

Fig. 6. Detection limits for MV^{2+}, quinine, and $Ru(bpy)_3^{2+}$ vs. i.d., of the nanotubes used in the sensor.

Table 1. Detection limits obtained for the three different electrode/electrolyte systems studied. Nanotubule i.d. = 2.8 nm.

Cell	Analyte	Detection limit (M)
Pt/KF	$Ru(bpy)_3^{2+}$	10^{-9}
Ag/AgCl/KCl	$Ru(bpy)_3^{2+}$	10^{-10}
	Quinine	10^{-8}
	MV^{2+}	10^{-6}
	2-Naphthol	10^{-6}
Ag/AgCl/KI	$Ru(bpy)_3^{2+}$	10^{-11}
	Quinine	10^{-8}
	MV^{2+}	10^{-7}
	2-Naphthol	10^{-6}

calibration plots. Figure 6 shows plots of detection limits for these three different analytes vs. the nanotube inside diameter in the membrane used. A minimum in this plot is observed for each of the three analytes.

The nanotube membrane that produces the minimum (best) detection limit depends on the size of the analyte. These molecules decrease in size in the order $Ru(bpy)_3^{2+}$ > quinine > MV^{2+}. The nanotube membrane that yields the lowest detection limit follows this size order; that is, the nanotube diameters that produce the lowest detection limit for $Ru(bpy)_3^{2+}$, quinine, and MV^{2+} are 2.8 nm, 2.2 nm, and 1.8 nm, respectively. For the roughly spherical analytes, the optimal tube diameter is a little over twice the diameter of the molecule.

6. Molecular Size Based Selectivity

The data presented above show a strong correlation between detection limit and the relative sizes of the nanotube and the analyte molecule (Figure 6). This indicates that this device should show molecular-size-based selectivity. This is not surprising given the transport studies discussed previously. To explore size-based selectivity, a series of solutions were prepared containing decreasing concentrations of the analyte species, but containing a constant (higher) concentration of an interfering species. The interfering species was smaller than the analyte species. The response of the nanotube membrane (nanotube diameter = 2.8 nm) to these solutions was then measured starting from lowest to highest concentration of the analyte species.

The small pyridine molecule was used as the first interfering species. When present at a concentration of 10^{-4} M, pyridine offered very little interference for any of the analytes $Ru(bpy)_3^{2+}$, MV^{2+} or quinine. The detection limits in the presence of 10^{-4} M pyridine were 10^{-10} M for $Ru(bpy)_3^{2+}$, 10^{-6} M for MV^{2+} and 10^{-7} M for quinine, within an order of magnitude of the detection limit with no added interfering species (Table 1). Put another way, this nanotube membrane sensor can detect 10^{-10} M $Ru(bpy)_3^{2+}$ in the presence of six orders of magnitude higher pyridine concentration.

A second set of experiments was done using the larger MV^{2+} as the interfering species. Now at low concentrations of analyte, there is a region where the device produces a constant response due to the constant concentration (10^{-4} M) of this interfering species; i.e., the much higher concentration of the MV^{2+} swamps the response of the device. However, as the concentration of $Ru(bpy)_3^{2+}$ increases, there is a concentration range where the device responds to this analyte species without interference from the MV^{2+}. This concentration range begins at concentrations of $Ru(bpy)_3^{2+}$ above 10^{-8} M. That is, the size-based selectivity is such that the larger analyte species, $Ru(bpy)_3^{2+}$, can be detected down to 10^{-8} M in the presence of four orders of magnitude higher concentration of the smaller interfering species, MV^{2+}.

For efficient bioseparation, higher selectivity along with higher flux is desirable. We will now discuss how to improve and tailor selectivity for protein separation using synthetic membranes [27b]. For separation of two or more proteins in a solution, the selectivity depends on various parameters including pH of the solution, molecular weight and shape of protein, and internal diameter of nanotubes. In general, the

bigger and heavier proteins move slower through solution compared to smaller proteins. Similarly, protein shape is also an important consideration. As discussed earlier selectivity of a particular is highly dependent upon internal diameter (i.d.) of the nanotubule membranes used. For example, molecules with size bigger than i.d. of nanotubules will be rejected, and will not pass through the membrane. The molecules smaller than i.d. will, however, pass through the membrane to permeate side. This sieving effect has been used previously to achieve very high selectivity [1]. Reducing diameter of the nanotubes to achieve higher selectivity generally leads to decrease in transport flux. Although selectivity achieved by synthetic nanotubule membranes is extraordinarily high, the flux is very low for practical considerations. This limitation can be alleviated by observing that proteins are charged biopolymers, and transmembrane potential can be used to augment protein transport by electrophoresis process. Depending upon pH of the solution, they can either be positive or negative charged. This factor can be very useful in increasing the flux without losing selectivity. For example, at pH 7, lysozyme is positively charged while bovine serum albumin (BSA) is negatively charged. By applying appropriate potential, the transport of one protein can be significantly enhanced while retarding the transport of other protein [27b]. Lastly, by optimizing parameters such as pH of the solution, i.d. of the nanotubes, and applied potential should enhance the selectivity significantly without sacrificing transport flux of the protein.

7. Synthetic Ion Channel Pores

We have conducted experiments that provide proof of the basic concept that an analyte molecule can switch on an ion current in a synthetic membrane-based ion-channel mimic [29]. The membrane used for most experiments was a commercially available microporous alumina filter. The pores in this membrane were made hydrophobic by reaction with an 18-carbon (C_{18}) alkyl silane. When placed between two salt solutions, the pores in this C_{18}-derivatized membrane are not wetted by water, yielding the "off" state of the membrane (Figure 1b). When exposed to a solution containing a sufficiently high concentration of a long chain ionic surfactant (the analyte), the surfactant molecules partition into the hydrophobic membrane, and ultimately cause the pores to flood with water and electrolyte (Figure 1b). As a result, the membrane will now support an ion current, and the ion channel-mimetic membrane is switched to its "on" state. Cationic drug molecules can also switch this membrane from the off to the on state (Figure 1b).

8. Membrane Preparation and AC Impedance Experiments with 1-Dodecanesulfonic Acid (DBS) Analyte

The alumina membranes were Anopore (Whatman Inc., Clifton, New Jersey) that had nominally 200 nm-diameter pores and were 60 μm thick. The alumina membranes were modified with octadecyltrimethoxysilane [29]. The membrane assembly was mounted between the halves of a U-tube permeation cell, and both half-cells were filled with ca. 20 mL of 0.1 M KCl. A Ag/AgCl working electrode was immersed into one half-cell solution, and a Pt counter electrode and a Ag/AgCl reference electrode were placed in the other half-cell [32, 33].

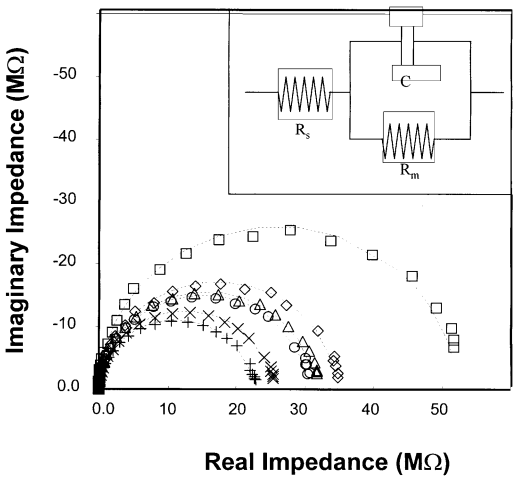

Fig. 7. Nyquist plots for a C18-modified alumina membrane upon exposure to increasing concentrations of DBS in 0.1 M KCl. The points are the experimental data. The lines are calculated data obtained using the equivalent circuit shown in the inset. Concentrations of DBS were as follows: □ 0 nM, ◇ 1.4 nM, △ 3 nM, ○ 10 nM, × 40 nM, + 100 nM.

AC impedance measurements proved to be a useful way to demonstrate the analyte-induced switching of the membrane between the off and on states. The upper-most curve in Figure 7 is the Nyquist plot for a C_{18}-modified alumina membrane with 0.1 M KCl solutions, and no analyte (DBS), on either side of the membrane (see also Figure 1b). As per prior investigations of ion-channel and ion-channel-mimetic membranes [34, 35] the impedance data were interpreted in terms of the equivalent circuit shown in the inset of Figure 7, where R_s is the solution resistance, R_m is the membrane resistance, and C is the membrane capacitance. The dashed curve is the best fit to the experimental data, from which the R_m (Figure 8) and C values were obtained. Also shown in Figure 7 are impedance data after spiking the half-cell electrolyte solutions to the indicated concentrations with the analyte (DBS).

In the absence of DBS, the membrane resistance is very large, >50 MΩ as opposed to ca. 5 Ω for the alumina membrane before modification with the C_{18} silane. Transport experiments (vide infra) show that this is because the very hydrophobic C_{18}-modified pores are not wetted by water. This is supported by contact angle measurements on the membrane surface, where a water contact angle of $130(\pm 8)^\circ$ was obtained for the C_{18}-treated alumina membrane as opposed to ca. $8(\pm 1)^\circ$ for the untreated membrane.

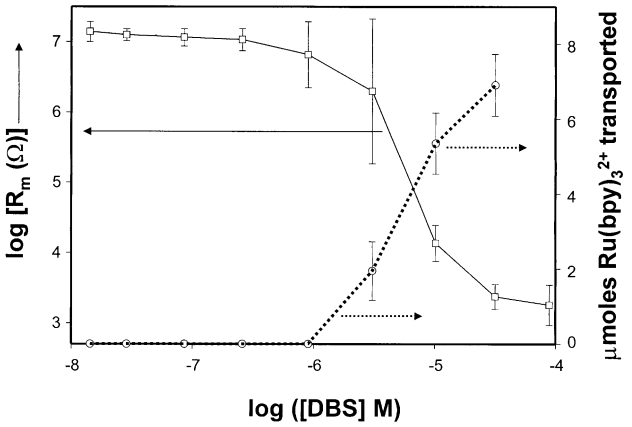

Fig. 8. Plots of log membrane resistance (left *y*-axis) and μmoles $Ru(bpy)_3^{2+}$ transported across the membrane (right *y*-axis) vs. log [DBS] for a C_{18}-modified alumina membrane. The error bars represent the standard deviation of three separate experiments.

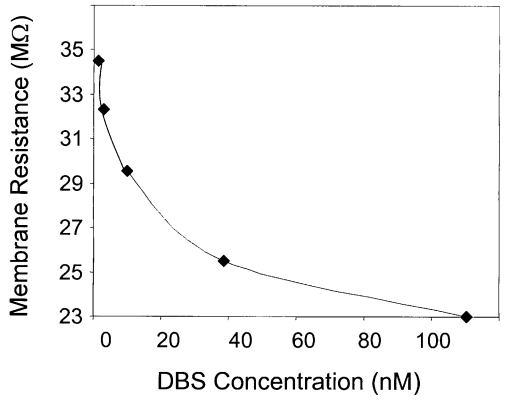

Fig. 9. Plot of membrane resistance vs. DBS concentration.

While over the concentration range 10^{-9} to 10^{-7} M there is some drop in membrane resistance with increasing DBS concentration (Figure 9), R_m remains very large (> 20 MΩ). However, over the DBS concentration range between 10^{-6} and 10^{-5} M there is a precipitous, four-order-of-magnitude, drop in R_m (Figure 8). This drop signals the analyte-induced switching of the membrane from the off to the on states.

9. Transport Experiments

These were conducted by mounting the membrane between the two halves of a U-tube permeation cell and adding 0.1 M KCl to each half-cell. The feed half-cell was also 50 μM in either $Ru(bpy)_3^{2+}$ or naphthalene disulfonate (NDS^{2-}), the permeate ions. An increment of the analyte surfactant (for these experiments DBS) was added to both the feed and permeate half-cells and permeation was allowed to occur for 24 hours. After this time, the permeate half-cell was sampled and the UV absorbance was used to determine the moles of the permeate ion transported. The permeate solution was then returned to the permeate half-cell and a second increment of DBS was added. Permeation was again allowed to occur for 24 hours and the amount of permeate ion transport was again determined. This process was repeated for various DBS concentrations over the range from 10^{-8} to 10^{-4} M.

The data obtained for $Ru(bpy)_3^{2+}$ transport are shown in Figure 8. At DBS concentrations below 10^{-6} M there is no detectable $Ru(bpy)_3^{2+}$ in the permeate solution. It is important to emphasize that each permeation data point in Figure 8 corresponds to an additional 24 hours of permeation time. Hence, by the time the DBS concentration was increased to 9×10^{-7} M, the total permeation time was 5 days. The inability to detect $Ru(bpy)_3^{2+}$ in the permeate solution after five days of permeation, shows that over the DBS concentration range 0 to ca. 10^{-6} M, the pores in the C_{18} membrane are not wetted by water, making the rate of $Ru(bpy)_3^{2+}$ transport immeasurable small. These data, again, show that at DBS concentrations below 10^{-6} M, the membrane is in the off state.

At DBS concentrations above 10^{-6} M, $Ru(bpy)_3^{2+}$ transport is switched on, and flux increases with concentration of DBS for concentrations above this value. The impedance and transport data tell a consistent story about the effect of DBS on the C_{18}-derivatized membrane (Figure 8). At low DBS concentrations ($< 10^{-6}$ M) where the membrane resistance is in the 10^7 ohm range, $Ru(bpy)_3^{2+}$ is not transported. The sudden drop in R_m at DBS concentrations above ca. 10^{-6} M is seen in the transport experiments as a abrupt switching on of $Ru(bpy)_3^{2+}$ transport across the membrane.

10. X-Ray Photoelectron Spectroscopy (XPS)

XPS was used to show that the prototypical analyte dodecylbenzene sulfonate (DBS) is present on the C_{18}-modified alumina surface after exposure of the membrane to DBS solution. However, the XPS cross-section for S from the DBS proved too weak to obtain unambiguous evidence; furthermore, O, C and Na^+ (the counterion for the DBS) are ubiquitous, and therefore not useful as probes to prove that DBS is present on the surface. For this reason, we used a surface ion exchange reaction to replace Na^+ with Cs^+ as the counterion for the surface-bound DBS. We then used XPS to look for the presence of Cs^+ on the C_{18}-modified surface that had been treated with DBS, using an identical surface that was exposed to the Cs^+ solution but not to DBS as the control.

Figure 10 shows XPS data for a C_{18}-modified membrane that had been exposed to an aqueous 2.0 mM solution of Na^+-DBS, rinsed, exposed to a 100 mM aqueous solution of $CsNO_3$, and then rinsed extensively again. The Cs 3d peaks at 724 and 738 eV are clearly evident [36]. This may be contrasted to the control surface – a C_{18}-modified alumina membrane that was exposed to the Cs^+ solution but not to DBS – where no Cs signal is seen (Figure 10). These data show that exposure of the membrane to DBS results in

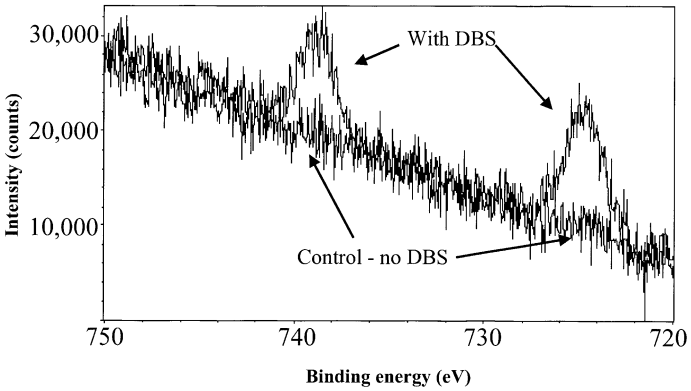

Fig. 10. XPS data for a C_{18}-modified alumina-membrane surface that was exposed to a DBS solution and then to a Cs^+ solution and for an identical surface that was exposed to Cs^+ but not to DBS.

partitioning of this analyte species onto the C_{18}-modified surface.

11. Measurements of Ion Current

While the transport experiments show that the analyte DBS can switch on ion (e.g., $Ru(bpy)_3^{2+}$ and NDS^{2-}) transport across the membrane, we also wanted to get a direct measure of the ion current. To do this, a constant transmembrane potential of 1.5 V was applied and the resulting transmembrane ion current was measured. The current was monitored for 30 min and then the half-cell solutions were spiked with DBS to a total concentration of 10^{-9} M. The current was again measured for 30 minutes and the half-cells were spiked again with DBS. This process was repeated for various DBS concentrations over the range from 10^{-9} to $10^{-3.5}$ M.

Figure 11 shows the measured ion current vs. time data; at the indicated times the electrolyte solutions were spiked to the indicated concentrations with DBS. The ion-current data show the same general trend as both the impedance and transport data – at concentrations below ca. 10^{-6} M the ion current is at a very low baseline value and at concentrations above ca. 10^{-6} M the ion current abruptly switches on. In addition, the $10^{-5.5}$ M datum shows that the transition from the low-current to the high-current state occurs very abruptly.

Both the impedance and ion-current data show that when the membrane is in the off state, some small baseline current does flow across the membrane. It is important to note that the resistance value for the off state obtained by the impedance and ion current measurements are essentially identical. As shown in Figure 7, the impedance measurement yields a value of ca. 10^7 Ω. The ion current in the off state is ca. 1.5×10^{-7} A, which for a 1.5 V transmembrane potential yields a membrane resistance of ca. 10^7 Ω. The issue left to resolve, however, is – what is supporting this baseline ion current when the membrane is in the off state? At this point we cannot say other than to suggest that this current results from some surface conduction process that occurs along the pore walls when the pores are devoid of water. In the absence of DBS, this surface conduction process may involve residual surface hydroxyl sites. The impedance data (Figure 7) indicate that in the presence of DBS, the surfactant itself is involved in the conduction process.

12. Detection of Drug Molecules

To explore the role of the hydrophobic effect in driving the analyte species into the C_{18}-derivatized alumina membrane, we investigated the effect of hydrophobic cationic drug

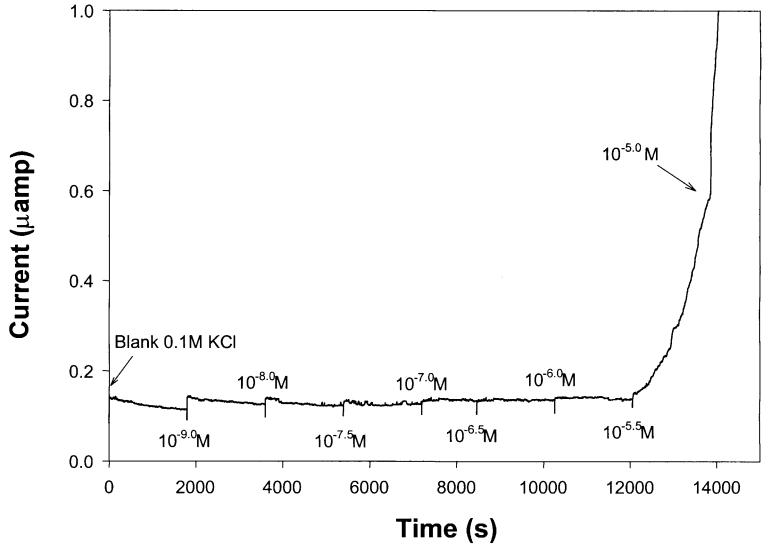

Fig. 11. Ion current through a C_{18}-modified alumina membrane vs. time. The contacting solution phases were spiked with the indicated concentrations of DBS at the indicated times. The electrolyte was 0.1 M KCl. A constant transmembrane potential of 1.5 V was applied.

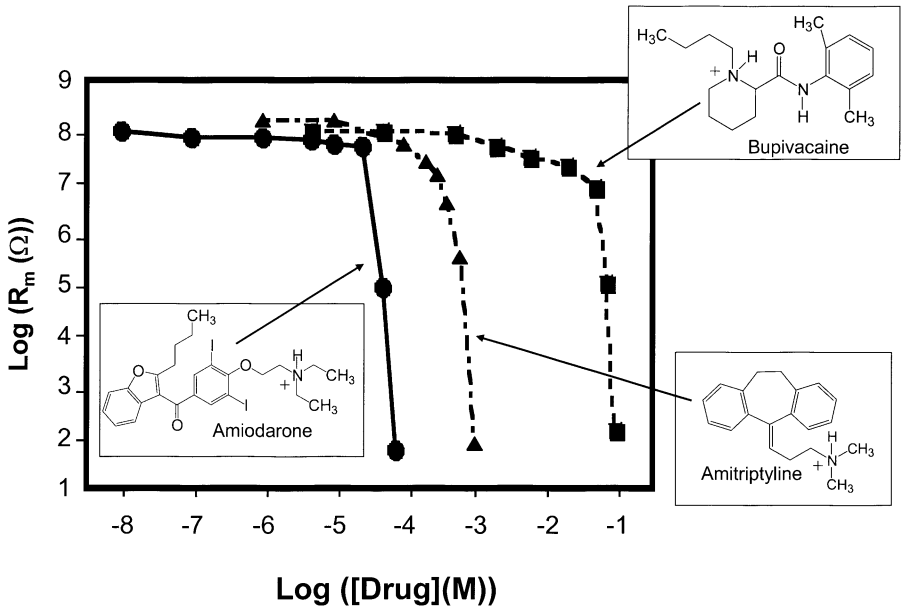

Fig. 12. Plots of log membrane resistance vs. log [Drug] for the indicated drugs and a C_{18}-modified alumina membrane.

molecules on the membrane resistance. The molecules and their molecular weights are amiodarone (645 g mol^{-1}), amitriptyline (278 g mol^{-1}), and bupivacaine (288 g mol^{-1}) (Figure 12). Because its molecular weight is more than double those of the other drugs and because it contains very hydrophobic iodo substituents, amiodarone is by far the most hydrophobic of these molecules. If the hydrophobic effect is responsible for driving molecules into the C_{18}-derivatized membrane, then the transition from the off to the on state would occur at lowest concentrations for amiodarone, and this is what is observed experimentally (Figure 12). There is only a 3% difference in the molecular weights of amitriptyline and bupivacaine; however, bupivacaine presents two additional opportunities for hydrogen bonding with water – the lone pairs on the carbonyl group and the lone pair of the non-protonated nitrogen. For this reason, bupivacaine is much more hydrophilic, and would be expected to be the most poorly detected of the three drugs; Figure 12 shows that this is also observed experimentally.

13. Conclusions

We have described highly-sensitive methods of electroanalysis based on Au nanotube membranes. In addition, we have also shown that synthetic micropore and nanotube membranes can mimic the function of ligand-gated ion channels; i.e., they can be switched from an off state to an on state in response to the presence of a chemical stimulus. This concept of ion-channel mimetic sensing, as originally proposed by Umezawa's group [37], has been of considerable interest in analytical chemistry [38–40]. These methods may find applications in protein separation, DNA purification, amplification and sequencing, and drug discovery. There is also considerable appeal in using naturally-occurring and genetically-engineered protein channels as sensors (see [41a] and references therein). Recently, we have fabricated ligand-gated ion-channel mimic micro-batteries [41b]. These batteries operate following application of an external chemical stimuli. Ion-channel batteries could find applications in bioanalytical and biomedical devices. Such research at the bio/nano interface is of great current interest in our group.

Now we will consider some of the limitations of electroanalysis methods discussed in this review. The response time of ligand-gated synthetic ion-channels is relatively low as compared to some other techniques presently used. An external chemical stimulus (i.e., a surfactant used in our case) is required for these devices to operate. The response time of measurements is limited by both diffusion coefficient as well as partition coefficient of chemical stimulus used for the process. The diffusion and partition coefficients of the surfactant would, respectively, determine the response time and the quantity of the surfactant needed to open the switch from an "off" position to an "on" position. In principle, both of these parameters can be adjusted by use a proper choice of surfactant and nanopores (i.e., i.d., length, surface charge and other physical parameters of the pores). Another issue for a successful device is its reversibility from "off" position to "on" and vice verse, i.e., the device should be robust and reliable. For a good device, one would like to switch back and forth from an "off" position to an "on" position many times during its lifetime. Although it is possible to switch back and forth from an "on" position to an "off" position, there is still room for improvement for techniques discussed in this review.

14. Acknowledgement

Aspects of this work were supported by the Office of Naval Research and the National Science Foundation.

15. References

[1] C. R. Martin, *Science* **1994**, *266*, 1961.
[2] J. C. Hulteen, C. R. Martin, *J. Mater. Chem.* **1997**, *7*, 1075.
[3] C. R. Martin, D. T. Mitchell, *Anal. Chem.* **1998**, *70*, 322A.
[4] R. L. Fleischer, P. B. Price, R. M. Walker, *Nuclear Tracks in Solids*, University of California Press: Berkeley. CA **1975.**
[5] G. L. Hornyak, C. J. Patrissi, C. R. Martin, *J. Phys. Chem B* **1997**, *101*, 1548.
[6] M. Nishizawa, V. P. Menon, C. R. Martin, *Science* **1995**, *268*, 700.
[7] K. B. Jirage, J. C. Hulteen, C. R. Martin, *Science* **1997**, *278*, 655.
[8] J. C. Hulteen, C.R Martin, *J. Amer. Chem. Soc.* **1998**, *120*, 6603.
[9] K.B Jirage, J. C. Hulteen, C. R. Martin, *Anal. Chem.* **1999**, *71*, 4913.
[10] Z. Hou, N. L. Abbott, P. Stroeve, *Langmuir* **2000**, *16*, 2401.
[11] G. Tourillon, L. Pontinnier, J. P. Levy, V. Langlais, *Solid-State Lett*. **2000**, *3*, 20.
[12] C. Schonenberger, B. M. I. van der Zande, L. G. J. Fokkink, M. Henry, C. Schmid, M. Kruger, A. Bachtold, R. Huber, H. Birk, U. Staufer, *J. Phys.Chem. B* **1997**, *101*, 5497.
[13] C. R. Martin, in *Handbook of Conducting Polymers*, 2nd ed. (Eds: J. R. Reynolds, T. Skotheim, R. Elsebaumer), New York, Marcel Dekker, **1997**, pp. 409 – 421.
[14] S. Demoustier-Champagne, P.-Y. Stavaux, *Chem. Mater*. **1999**, *11*, 829.
[15] S. Sukeerthi, Q. Contractor, *Anal. Chem.* **1999**, *71*, 2231.
[16] B. B. Lakshmi, C. J. Patrissi, C. R. Martin, *Chem. Mater.* **1997**, 9, 2544.
[17] B. B. Lakshmi, P. K. Dorhout, C. R. Martin, *Chem. Mater.* **1997**, *9*, 857.
[18] G. Che, B. B Lakshmi, C. R. Martin, E. R. Fisher, *Langmuir* **1999**, *15*, 750.
[19] G. Che, E. R. Fisher, C. R. Martin, *Nature* **1998**, *393*, 346.
[20] C. J. Patrissi, C. R. Martin, *J. Electrochem. Soc.* **1999**, *146*, 3176.
[21] N. Li, C. J. Patrissi, C. R. Martin, *J. Electrochem. Soc.* **2000**, *147*, 2044.
[22] G. Che, K. B. Jirage, E. R. Fisher, C. R. Martin, H. Yoneyama, *J. Electrochem. Soc*. **1997**, *144*, 4296.
[23] V. M. Cepak, J. C. Hulteen, G. Che, K. B. Jirage, B. B. Lakshmi, E. R. Fisher, C. R. Martin, *J. Mater.Res.* **1998**, *13*, 3070.
[24] V. M. Cepak, J. C. Hulteen, G. Che, K. B. Jirage, B. B. Lakshmi, E. R. Fisher, C. R. Martin, *Chem. Mater*. **1997**, *9*, 1065.
[25] B. R. Martin, D. J. Dermody, B. D. Reiss, M. Fang, L. A. Lyon, M. J. Natan, T. E. Mallouk, *Adv. Mater*. **1999**, *11*, 1021.
[26] Y. Kobayashi, C. R. Martin, *Anal. Chem.* **1999**, *71*, 3665.
[27] Y. Kobayashi, C. R. Martin. *J. Electroanal. Chem.* **1997**, *431*, 29; S. Yu, S. B. Lee, C. R. Martin, *Anal. Chem.* **2003**, *75*, 1239; P. Kohli, S. E. Miller, R. Gasprac, C. R. Martin, in press.
[28] D. Voet, J. G. Voet, *Biochemistry*, 2nd ed., Wiley, New York **1995**, pp. 1297 – 1298.
[29] E. D. Steinle, D. T. Mitchell, M. Wirtz, S. B. Lee, V. Y. Young, C. R. Martin, *Anal. Chem.* **2002**, *74*, 2416.
[30] V. P. Menon, C. R. Martin, *Anal. Chem.* **1995**, *67*, 1920.
[31] M. Kang, C. R. Martin, *Langmuir* **2001**, *17*, 2753.
[32] R. D. Armstrong, A. K. Covington, G. P. Evans, *J. Electroanal. Chem.* **1983**, *159*, 33.
[33] S. L. Xie, K. Cammann, *J. Electroanal. Chem.* **1987**, *229*, 249.
[34] W. Zhang, U. E. Spichiger, *Electrochem. Acta* **2000**, *45*, 2259.
[35] L. Ding, J. Li, S. Dong, E. Wang, *J. Electroanal. Chem.* **1996**, *416*, 105.
[36] *Handbook of X-Ray Photoelectron Spectroscopy* (Ed: G. E. Muilenerg), Perkin-Elmer Corporation, Eden Prarie **1978.**
[37] M. Sugawara, K. Kojima, H. Sazawa, Y. Umezawa, *Anal. Chem*. **1987**, *59*, 2842.
[38] K. P. Xiao, P. Bühlmann, Y. Umezawa, *Anal. Chem.* **1999**, *71*, 1183.
[39] Z. Wu, J. Tang, Z. Cheng, X. Yang, E. Wang, *Anal. Chem.* **2000**, *72*, 6030.
[40] Y. Katayama, Y. Ohuchi, X. Yang, E. Wang, *Anal. Chem.* **2000**, 4671.
[41] H. Bayley, C. R. Martin, *Chem. Rev., Sensors Thematic Issue*, **2000**, *100*, 2575; L. Trofin, S. B. Lee, D. T. Mitchell, C. R. Martin, in press.

